nature photonics

LETTERS

PUBLISHED ONLINE: 27 SEPTEMBER 2009 | DOI: 10.1038/NPHOTON.2009.166

# Excitonic switches operating at around 100 K

G. Grosso[1], J. Graves[1], A. T. Hammack[1], A. A. High[1]*, L. V. Butov[1], M. Hanson[2] and A. C. Gossard[2]

**Photonic and optoelectronic devices may offer the opportunity to realize efficient signal processing at speeds higher than in conventional electronic devices. Switches form the building blocks for circuits, and fast photonic switches have been realized[1–6]. Recently, a proof of principle demonstration of exciton optoelectronic devices was reported[7,8]. The potential advantages of excitonic devices include high operation and interconnection speed, small dimensions and the opportunity to combine many elements into integrated circuits. Here, we demonstrate experimental proof of principle for the operation of excitonic switching devices at temperatures around 100 K. The devices are based on an AlAs/GaAs coupled quantum well structure and include the exciton optoelectronic transistor (EXOT), the excitonic bridge modulator (EXBM), and the excitonic pinch-off modulator (EXPOM). A two orders of magnitude increase in the operation temperature compared to earlier devices (1.5 K; refs 7,8) is achieved.**

The principle of operation of excitonic devices is based on the control of exciton fluxes by electrode voltages[7,8], and such devices may have photonic or excitonic inputs and outputs. In the former case, photons transform into excitons at the input and excitons transform into photons at the output[7]. In the latter case, excitons arrive at the input from (depart from the output to) another excitonic device[8]. The potential advantages of excitonic devices are briefly discussed below.

The first advantage is high interconnection speed. Efficient signal communication uses photons. Conventional signal processing, however, uses an optically inactive medium, electrons. An interconnection between electronic signal processing and optical communication causes a delay, thus slowing down the operation speed[9]. In contrast, excitons form a medium that can be used for signal processing and, at the same time, directly link to optical communication. Therefore, the delay between signal processing and optical communication is effectively eliminated in excitonic devices. This can provide a significant advantage in applications where the interconnection speed is important. The switching time combined with the interconnection time for the first proof-of-principle excitonic transistor was ~0.2 ns (ref. 7), close to ultrafast photonic modulators.

The second advantage is compactness and scalability. Photonic devices demonstrate fast operation speeds; however, the achievement of photonic signal modulation by a control gate usually requires large device dimensions that make the creation of compact circuits with many elements challenging[10]. The smallest dimensions achieved for Mach–Zehnder modulators are ~100 μm (refs 1–6). In comparison, excitonic transistors have an architecture and operation principle similar to electronic field-effect transistors (FET). Therefore, excitonic circuits have the potential to be similarly compact and can include as many elements as electronic circuits. The diffraction limit for the dimensions of excitonic devices is given by the exciton de Broglie wavelength, and is much smaller than the diffraction limit for the dimensions of photonic devices given by the wavelength of light (the exciton thermal de Broglie wavelength scales with temperature in proportion to $T^{-1/2}$ and is ~10 nm at room temperature). In the first proof-of-principle excitonic transistor the distance between the source and drain was 3 μm (ref. 7) (limited by the resolution of the lithography used for the sample processing), which is considerably smaller than the dimensions of photonic devices. The proof of principle for the integration of excitonic transistors into circuits has been demonstrated in ref. 8.

The major challenges for excitonic devices are finite exciton lifetime and finite exciton binding energy. In a regular direct-gap semiconductor, the exciton lifetime is typically less than a nanosecond, allowing the exciton to travel only a small distance before it recombines. This problem is addressed by using indirect excitons composed of electrons and holes in separated layers[7,8]. The lifetime of indirect excitons exceeds by orders of magnitude the lifetime of regular excitons and increases exponentially with the separation $d$ between the layers and the height of the separating barrier. Within their lifetime, indirect excitons can travel over large distances[11–17] for which devices can be readily patterned.

A finite exciton binding energy $E_{ex}$ limits the operation temperature. Excitons exist in the temperature range roughly below $E_{ex}/k_B$ (ref. 18; $k_B$ is the Boltzmann constant). The proof of principle of excitonic devices was carried out at 1.5 K in a $GaAs/Al_{0.33}Ga_{0.67}As$ coupled quantum well structure (CQW) with $d = 12$ nm and where $E_{ex}/k_B \approx 40$ K (refs 7,8). Increasing the operation temperature requires different materials and architectures. The goal is to create efficient excitonic devices that are operational at room temperature. Note that materials with a large $E_{ex}$ include wide-bandgap semiconductors[19] and organic materials[20].

Here, we report on a proof of principle for the operation of excitonic switches at $T \approx 100$ K. This is a two orders of magnitude increase in the operation temperature compared to the earlier devices, where operation was demonstrated at 1.5 K (refs 7,8). It shows that the operation of excitonic devices is not limited to liquid helium temperatures. The devices are based on AlAs/GaAs CQW (Fig. 1a). A small $d \approx 3$ nm results in a high binding energy of indirect excitons in such CQW $E_{ex}/k_B \approx 100$ K (ref. 21), permitting device operation at elevated temperatures.

We first study exciton transport along and across a 10-μm-wide electrode. At zero applied voltage $V$, indirect excitons form the lowest energy state in this structure[21]. Application of a positive (negative) $V$ increases (lowers) the exciton energy by $edF_z$ ($F_z$ is the electric field in the $z$-direction)[22]. The linear electrode creates a channel for indirect excitons at negative $V$ (Fig. 1b) and an anti-channel at positive $V$ (Fig. 1c). Figures 1d,h show the exciton cloud confinement in the channel. Excitons spread beyond the channel at higher densities (Fig. 1h) due to the screening of the confining potential by the excitons[23]. Figure 1e,i shows the exciton cloud spreading away from the anti-channel. The exciton emission reaches a maximum intensity a few micrometres away from the anti-channel (the emission profiles in Fig. 1f–i are corrected for the electrode absorption). Both the increased exciton density away from the potential energy hill of the

[1]Department of Physics, University of California at San Diego, La Jolla, California 92093-0319, USA, [2]Materials Department, University of California at Santa Barbara, Santa Barbara, California 93106-5050, USA. *e-mail: alex.high@gmail.com

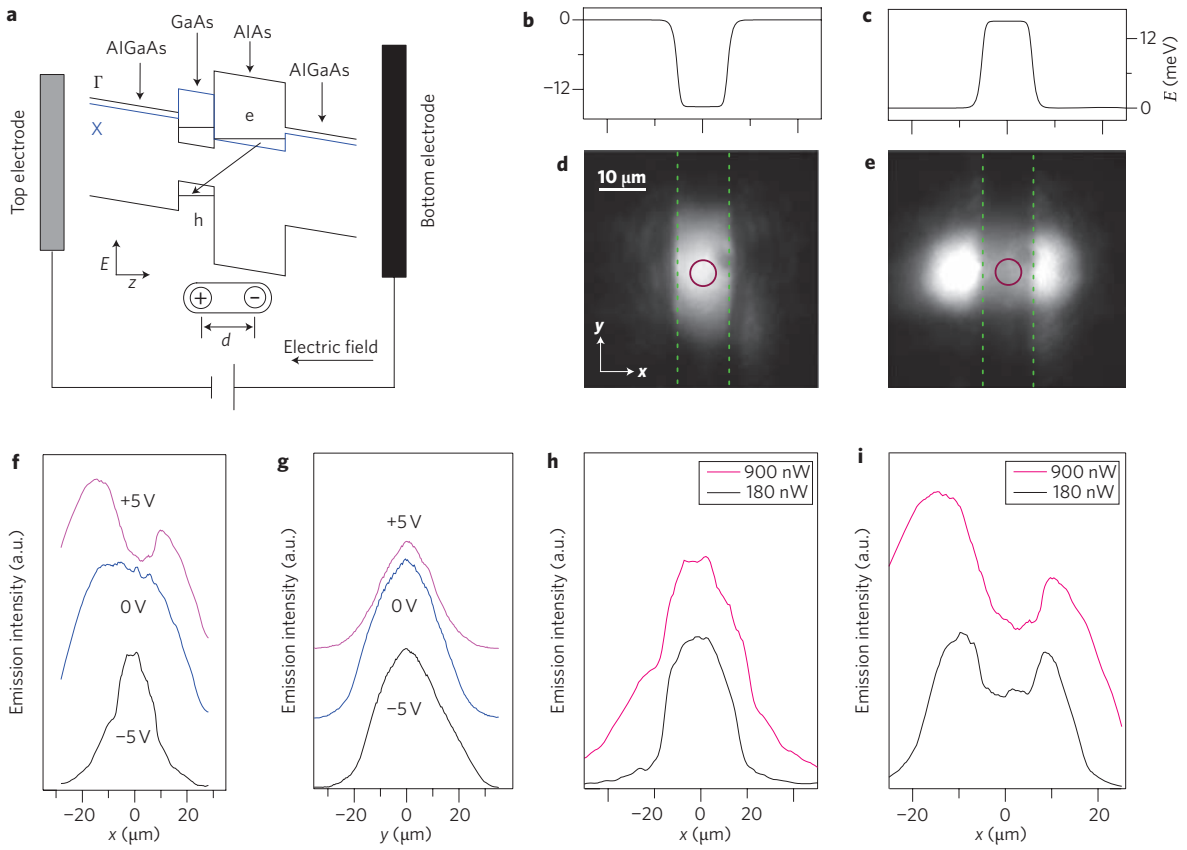


**Figure 1 | Indirect excitons in electrostatic channels and anti-channels. a**, Schematic band diagram for an AlAs/GaAs coupled quantum well structure (CQW); e, electron; h, hole. **b**,**c**, Calculated exciton energy profiles for the channel at $V = -5$ V (**b**) and the anti-channel at $V = +5$ V (**c**) produced by voltage $V$ applied to a linear 10-μm-wide 90-μm-long electrode. **d**,**e**, Image of the exciton cloud confined in the channel (**d**) and spreading from the anti-channel (**e**) for excitation density $P = 180$ nW. The electrode edges are indicated by the dashed lines. The circle shows the position of the laser excitation. **f**,**g**, Emission intensity profiles across (**f**) and along (**g**) the electrode for $V = -5$, 0, and +5 V at $P = 900$ nW. **h**,**i**, Emission intensity profiles in the channel (**h**) and the anti-channel (**i**) for $P = 180$ and 900 nW. $T = 6$ K for all data.

anti-channel and the increased occupation of the optically active exciton states with momenta $k \leq k_0 \approx E_g\sqrt{\varepsilon}/(\hbar c)$ ($E_g$ is the bandgap, $\varepsilon$ is the dielectric constant) due to exciton relaxation to $k \leq k_0$ states away from the excitation spot at the potential energy hill contribute to the observed intensity increase beyond the anti-channel. The latter mechanism was suggested as an explanation of the exciton rings in refs 14 and 17. Figure 1h shows the transition from a channel to an anti-channel with increasing $V$. The confining potential of the channel or potential energy hill of the anti-channel strongly affect the exciton transport in the $x$-direction and relatively weakly affect it in the $y$-direction (Fig. 1f,g). The latter presents the characteristic transport length $l_{ex}$ of indirect excitons in the structure.

Figure 1 shows that $l_{ex}$ is large enough that excitons can travel over distances exceeding the dimensions of excitonic devices. $l_{ex}$ reduces with increasing temperature (Fig. 2a,b). At high temperatures, the largest $l_{ex}$ is observed around $V \approx 1$ V (Fig. 2a). These data are consistent with earlier data on exciton lifetime $\tau$ in AlAs/GaAs CQW: $\tau$ reduces (1) at positive $V$ as a result of approaching the direct regime, (2) at negative $V$ because of the escape of electrons and holes from the CQW through the reduced barrier, and (3) at high temperatures as a result of increased non-radiative recombination[12,24], and the reduction of $\tau$ results in the reduction of $l_{ex} \sim \sqrt{(D\tau)}$ ($D$ is the exciton diffusion coefficient).

Figure 3 presents the proof of principle for the operation of the exciton optoelectronic transistor (EXOT) at 85 K. The operation principle of the EXOT is similar to that of an electronic FET[7,8]. The EXOT is a three-terminal device in which the exciton flux

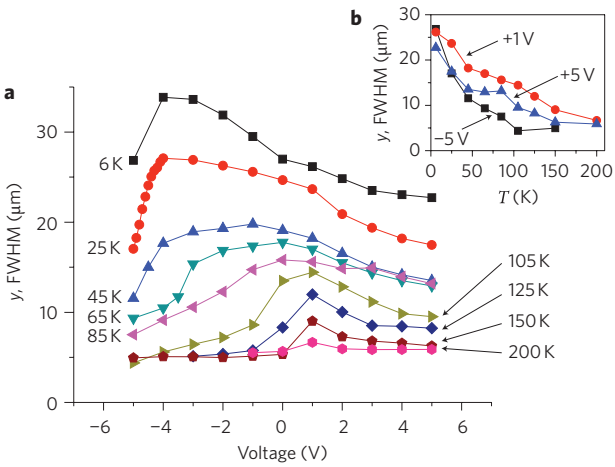


**Figure 2 | Transport length of indirect excitons in the AlAs/GaAs CQW.** **a**,**b**, The size (FWHM) of the exciton cloud along the linear electrode versus electrode voltage $V$ for different temperatures (**a**) and versus temperature for different $V$ (**b**) at $P = 900$ nW.

between two electrodes is controlled by a voltage applied to the third electrode. Here, the EXOT operates in switching mode. The excitons are excited at the source (input) and travel to the drain (output) because of the potential energy gradient $\sim ed(F_{zd} - F_{zs}) \propto (V_d - V_s)$ created by the source voltage $V_s$ and drain voltage $V_d$.

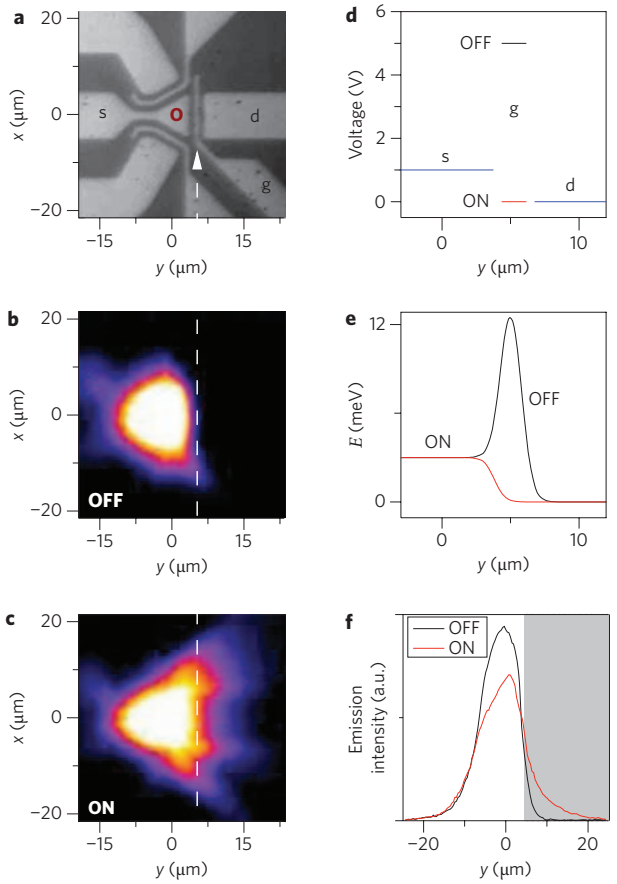


**Figure 3 | EXOT operation at 85 K. a**, Electrode pattern. The circle shows the position of the laser excitation. The exciton flux from source electrode s to drain electrode d is controlled by a gate electrode g, the position of which is indicated by a dashed line. **b**,**c**, Images of the EXOT emission in on and off states at $T = 85$ K, $P = 450$ nW. **d**,**e**, Voltages (**d**) and calculated single-exciton energy profiles (**e**) in on and off states. $V_s = 1$, $V_d = 0$, $V_g = 0$ in the on state and 5 V in the off state, and the voltage applied to the rest of the electrodes is 5 V. **f**, Emission intensity along the exciton flux for on (red line) and off (black line) states corresponding to the false-colour images in **b** and **c**. The grey area indicates the drain region.

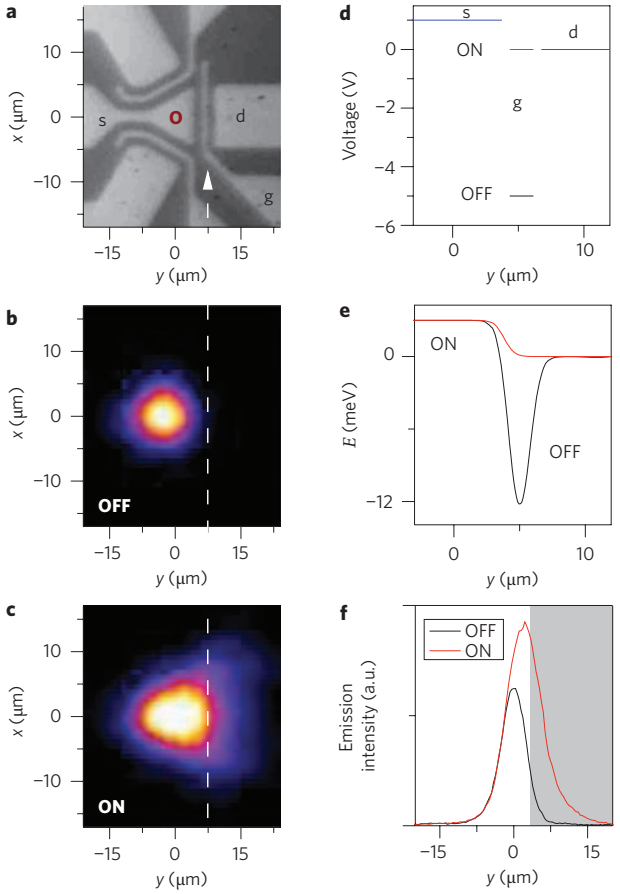


**Figure 4 | EXBM operation at 125 K. a**, Electrode pattern. The circle shows the position of the laser excitation. The exciton flux from source electrode s to drain electrode d is controlled by a gate electrode g, the position of which is indicated by the dashed line. **b**,**c**, Images of the EXBM emission in off and on states at $T = 125$ K, $P = 4.5$ μW. **d**,**e**, Voltages (**d**) and calculated single-exciton energy profiles (**e**) in on and off states. $V_s = 1$, $V_d = 0$, $V_g = 0$ in the on state and −5 V in the off state, and the voltage applied to the rest of the electrodes is −5 V. **f**, Emission intensity along the exciton flux for on (red line) and off (black line) states corresponding to the false-colour images in **b** and **c**. The grey area indicates the drain region.

The exciton flux from source to drain is controlled by a gate voltage $V_g$, which creates (removes) a barrier in the region of the gate electrode when the EXOT is off (on) (see Fig. 3d,e). The emission images for the EXOT in both the off state and on state are shown in Fig. 3b,c. The on/off ratio of the signal integrated over EXOT output (shaded region) reaches 5 (Fig. 3f).

Exciton flux modulations can also be achieved by other configurations of electrode voltages. Figure 4 presents the proof of principle for the operation of the excitonic bridge modulator (EXBM) at 125 K. In this device, the exciton flux from source to drain is terminated in the off state by a considerable reduction of the exciton lifetime in the gate region. This is achieved by applying a large negative voltage to the gate electrode, which increases the carrier escape out of the CQW in the $z$-direction in the gate region[24]. In turn, the exciton flux can flow from source to drain when the gate electrode provides a bridge between the source and drain with a long exciton lifetime. The on/off ratio of the signal integrated over the EXBM output (shaded region) reaches 9 (Fig. 4f).

Figure 5 presents the proof of principle for the operation of the excitonic pinch-off modulator (EXPOM) at 85 K. In this device, the exciton flux through the 2 μm constriction in the electrode—the channel—is controlled by varying the voltage on the laterally adjacent electrodes $V_a$. Increasing $V_a$ narrows the channel and also increases the exciton energy in the channel (Fig. 5e,g), reducing the exciton flux through it. The EXPOM is similar to split-gate electronic devices. The on/off ratio of the signal integrated over the area right of the channel (shaded region) reaches 12 (Fig. 5f).

At high temperatures, ~100–150 K, the exciton transport length becomes small compared to the device dimensions (Fig. 2), $E_{ex}/k_B$ becomes comparable to the temperature, and the on/off ratio for the switches in the AlAs/GaAs CQW vanishes. The optimization of excitonic devices is the subject of ongoing research.

## Methods

The structure was grown by molecular beam epitaxy. An $n^+$-GaAs layer with $n_{Si} = 10^{18}$ cm$^{-3}$ served as an homogeneous bottom electrode. The top electrodes were fabricated by depositing a semi-transparent layer of platinum (8 nm) and gold (2 nm). The 2.5-nm GaAs QW and 4-nm AlAs QW were positioned 0.1 μm above the $n^+$-GaAs layer within an undoped 1-μm-thick $Al_{0.45}Ga_{0.55}$ As layer. Positioning the CQW closer to the homogeneous electrode suppresses the in-plane electric field[25], which can otherwise lead to exciton dissociation. Additional information on the device structure is available in the Supplementary Information. Excitons were photoexcited by a 633-nm HeNe laser within a 4-μm FWHM (full-width at half-maximum) spot. The emission images were taken by a charge-coupled device camera with an interference filter covering the spectral range of the indirect excitons emitting in the vicinity of 690 nm or using a spectrometer with a resolution 0.4 meV.

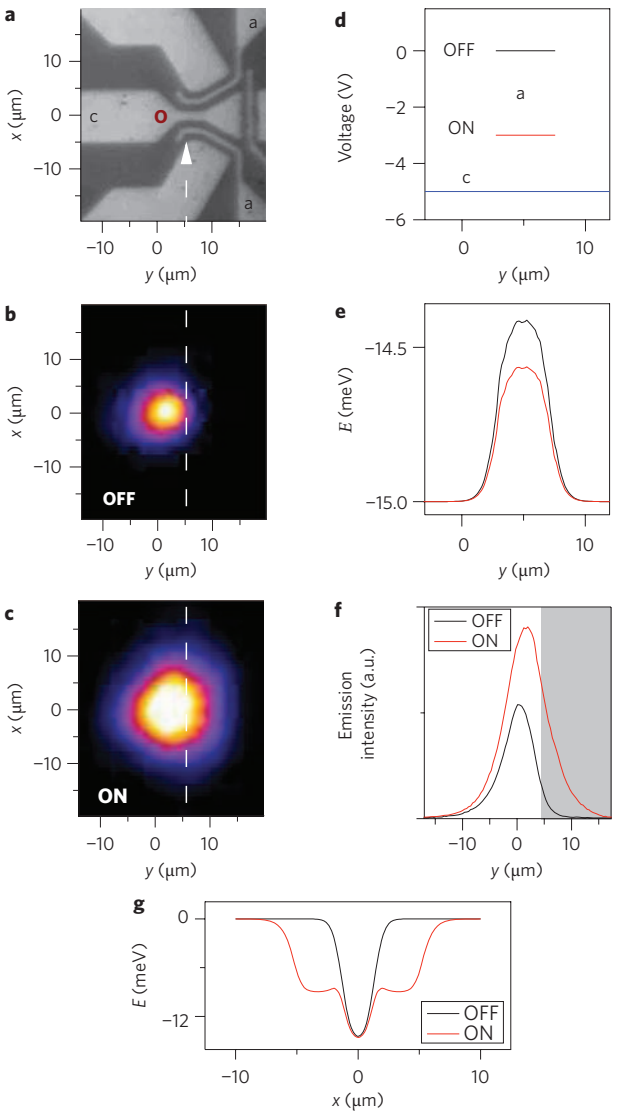


**Figure 5 | EXPOM operation at 85 K. a**, Electrode pattern. The circle shows the position of the laser excitation. The exciton flux through the constriction in channel electrode c, the position of which is indicated by a dashed line, is controlled by the voltage on adjacent electrodes a. **b**,**c**, Images of the EXPOM emission in on and off states at $T = 85$ K, $P = 6.3$ μW. **d**,**e**,**g**, Voltages (**d**) and calculated single-exciton energy profiles in on and off states in $x$ (**g**) and $y$ (**e**) directions. $V_c = -5$, $V_a = -3$ V in the on state and 0 V in the off state, and the voltage applied to the rest of the electrodes is 0 V. **f**, Emission intensity along the exciton flux for on (red line) and off (black line) states corresponding to the false-colour images in **b** and **c**. The grey area indicates the region right of the channel.

The spatial resolution was 1.5 μm. The single-exciton energy profiles were calculated as in ref .25.

Received 22 June 2009; accepted 11 August 2009; published online 27 September 2009

## References

1. Liu, A. *et al.* A high-speed silicon optical modulator based on a metal-oxide-semiconductor capacitor. *Nature* **427,** 615–618 (2004).
2. Xu, Q., Schmidt, B., Pradhan, S. & Lipson, M. Micrometre-scale silicon electro-optic modulator. *Nature* **435,** 325–327 (2005).
3. Jiang, Y., Jiang, W., Gu, L., Chen, X. & Chen, R. T. 80-micron interaction length silicon photonic crystal waveguide modulator. *Appl. Phys. Lett.* **87,** 221105 (2005).
4. Green, W. M. J., Rooks, M. J., Seekaric, L. & Vlasov Y.A. Ultra-compact, low RF power, 10 Gb/s silicon Mach–Zehnder modulator. *Opt. Express* **15,** 17106–17113 (2007).
5. Liu, J. *et al.* Waveguide-integrated, ultralow-energy GeSi electro-absorption modulators. *Nature Photon.* **2,** 433–437 (2008).
6. Chen, H. W., Kuo, Y. H. & Bowers, J. E. High speed hybrid silicon evanescent Mach–Zehnder modulator and switch. *Opt. Express* **16,** 20571–20576 (2008).
7. High, A. A., Hammack, A. T., Butov, L. V., Hanson, M. & Gossard, A. C. Exciton optoelectronic transistor. *Opt. Lett.* **32,** 2466–2468 (2007).
8. High, A. A., Novitskaya, E. E., Butov, L. V., Hanson, M. & Gossard, A.C. Control of exciton fluxes in an excitonic integrated circuit. *Science* **321,** 229–231 (2008).
9. Miller, D. A. B. Rationale and challenges for optical interconnects to electronic chips. *IEEE* **88,** 728–749 (2000)
10. Wakita, K. *Semiconductor Optical Modulators* (Kluwer Academic Publishers, 1998).
11. Hagn, M., Zrenner, A., Böhm, G. & Weimann, G. Electric-field-induced exciton transport in coupled quantum well structures. *Appl. Phys. Lett.* **67,** 232–234 (1995).
12. Butov, L. V. & Filin, A. I. Anomalous transport and luminescence of indirect excitons in AlAs/GaAs coupled quantum wells as evidence for exciton condensation. *Phys. Rev. B* **58,** 1980–2000 (1998).
13. Larionov, A. V., Timofeev, V. B., Hvam, J. & Soerensen, K. Interwell excitons in GaAs/AlGaAs double quantum wells and their collective properties. *Sov. Phys. JETP* **90,** 1093–1104 (2000).
14. Butov, L. V., Gossard, A. C. & Chemla, D. S. Macroscopically ordered state in an exciton system. *Nature* **418,** 751–754 (2002).
15. Vörös, Z., Balili, R., Snoke, D. W., Pfeiffer, L. & West, K. Long-distance diffusion of excitons in double quantum well structures. *Phys. Rev. Lett.* **94,** 226401 (2005).
16. Gartner, A., Holleithner, A. W., Kotthaus, J. P. & Schul, D. Drift mobility of long-living excitons in coupled GaAs quantum wells. *Appl. Phys. Lett.* **89,** 052108 (2006).
17. Ivanov, A. L., Smallwood, L. E., Hammack, A. T., Sen Yang, Butov, L. V. & Gossard, A. C. Origin of the inner ring in photoluminescence patterns of quantum well excitons. *Europhys. Lett.* **73,** 920–926 (2006).
18. Chemla, D. S., Miller, D. A. B., Smith, P. W., Gossard, A. C. & Wiegmann, W. Room temperature excitonic nonlinear absorption and refraction in GaAs/AlGaAs multiple quantum well structures. *IEEE J. Quantum Electron.* **20,** 265–275 (1984).
19. Makino, T., Segawa, Y., Kawasaki, M. & Koinuma, H. Optical properties of excitons in ZnO-based quantum well heterostructures. *Semicond. Sci. Technol.* **20,** S78–S91 (2005).
20. Segal, M., Singh, M., Rivoire, K., Difley, S., Van Voorhis, T. & Baldo, M. A. Extrafluorescent electroluminescence in organic light-emitting devices. *Nature Mater.* **6,** 374–378 (2007).
21. Zrenner, A. *Festkörperprobleme/Advances in Solid State Physics.* Vol. 32, p. 61 (Vieweg, Braunschweig, 1992).
22. Miller, D. A. B. *et al.* Electric field dependence of optical absorption near the band gap of quantum-well structures. *Phys. Rev. B* **32,** 1043–1060 (1985).
23. Remeika, M. *et al.* Localization–delocalization transition of indirect excitons in lateral electrostatic lattices. *Phys. Rev. Lett.* **102,** 186803 (2009).
24. Butov, L. V., Zrenner, A., Abstreiter, G., Böhm, G. & Weimann, G. Condensation of indirect excitons in coupled AlAs/GaAs quantum wells. *Phys. Rev. Lett.* **73,** 304–307 (1994).
25. Hammack, A. T. *et al.* Excitons in electrostatic traps. *J. Appl. Phys.* **99,** 066104 (2006).

## Acknowledgements

This work was supported by ARO and NSF.

## Author contributions

All authors contributed to the work presented in this paper.

## Additional information

Supplementary information accompanies this paper at www.nature.com/naturephotonics. Reprints and permission information is available online at http://npg.nature.com/reprintsandpermissions/. Correspondence and requests for materials should be addressed to A.A.H.